Generalized Multiscale Finite Element Methods. Oversampling Strategies

Yalchin Efendiev[1,2*], **Juan Galvis**[2,3], **Guanglian Li**[2] **and Michael Presho**[2]

[1] *Center for Numerical Porous Media (NumPor)*
King Abdullah University of Science and Technology (KAUST)
Thuwal 23955-6900, Kingdom of Saudi Arabia.

[2] *Department of Mathematics & Institute for Scientific Computation (ISC)*
Texas A&M University
College Station, Texas, USA

[3] *Departamento de Matemáticas*
Universidad Nacional de Colombia
Bogotá D.C., Colombia

Abstract

In this paper, we propose oversampling strategies in the Generalized Multiscale Finite Element Method (GMsFEM) framework. The GMsFEM, which has been recently introduced in [12], allows solving multiscale parameter-dependent problems at a reduced computational cost by constructing a reduced-order representation of the solution on a coarse grid. The main idea of the method consists of (1) the construction of snapshot space, (2) the construction of the offline space, and (3) construction of the online space (the latter for parameter-dependent problems). In [12], it was shown that the GMsFEM provides a flexible tool to solve multiscale problems with a complex input space by generating appropriate snapshot, offline, and online spaces. In this paper, we develop oversampling techniques to be used in this context (see [19] where oversampling is introduced for multiscale finite element methods). It is known (see [19]) that the oversampling can improve the accuracy of multiscale methods. In particular, the oversampling technique uses larger regions (larger than the target coarse block) in constructing local basis functions. Our motivation stems from the analysis presented in this paper which show that when using oversampling techniques in the construction of the snapshot space and offline space, GMsFEM will converge independent of small scales and high-contrast under certain assumptions. We consider the use of multiple eigenvalue problem to improve the convergence and discuss their relation to single spectral problems that use oversampled regions. The oversampling procedures proposed in this

---

*Email address: efendiev@math.tamu.edu

paper differ from those in [19]. In particular, the oversampling domains are partially used in constructing local spectral problems. We present numerical results and compare various oversampling techniques in order to complement the proposed technique and analysis.

Keywords: Generalized multiscale finite element method, oversampling, high-contrast

1. Introduction

Heterogeneous media with multiple scales and high-contrast commonly occur in many applications, such as porous media and material sciences. The development of reduced-order models describing complex processes in such media is needed in such applications. There are a variety of multiscale methods, e.g. [1, 3, 16, 19–21], that efficiently capture multiscale behavior by constructing a reduced representation of the solution space on a coarse grid. While standard multiscale methods have proven effective for a variety of applications (see, e.g., [15–17, 21]), in this paper we consider a more recent framework, GMsFEM, in which the coarse spaces may be systematically enriched to converge to the fine grid solution. In particular, we develop oversampling techniques within GMsFEM and show that these methods converge independent of the small scales and high contrast under certain assumptions.

The Generalized Multiscale Finite Element Method (GMsFEM) is a flexible framework that generalizes the Multiscale Finite Element Method (MsFEM) by systematically enriching the coarse spaces and taking into account small scale information and complex input spaces. This approach, as in many multiscale model reduction techniques, divides the computation into two stages: offline and online. In the offline stage, a small dimensional space is constructed that can be efficiently used in the online stage to construct multiscale basis functions. These multiscale basis functions can be re-used for any input parameter to solve the problem on a coarse grid. The main idea behind the construction of offline and online spaces is the selection of local spectral problems and the selection of the snapshot space. In [12], we propose several general strategies. In this paper, our focus is on the development of oversampling strategies.

Oversampling techniques have been developed in the context of multiscale finite element methods [19] as well as upscaling methods [9]. These techniques use the local solutions in larger domains to construct multiscale basis functions in the context of MsFEM. We borrow that main concept in this paper. In particular, we use the space of snapshots in the oversampled regions by constructing a snapshot space spanned by harmonic functions or dominant eigenvectors of a local spectral problem formulated in the oversampled domain. Furthermore, we use special local spectral problems to determine the dominant modes in the space of snapshots. This spectral problem is motivated by the analysis and it uses a weighted mass matrix in the oversampled region while

the energy (stiffness) matrix is constructed in the target coarse domain. By choosing the dominant modes, we identify multiscale basis functions. These basis functions are then multiplied by partition of unity functions to solve the flow equation on a coarse grid (in the absence of the parameter). We also describe the use of multiple local spectral problems for enhancing the accuracy of the approximation and discuss their relation to single spectral problems that use oversampled regions where the latter provides an optimal space. In the presence of the parameter, we also design an online space following the same strategy as the offline space construction (but using an online parameter value). We employ the Galerkin finite element method, though discontinuous Galerkin methods can also be used [10].

We present numerical results that demonstrate the convergence of the proposed methods. In our numerical experiments, we test two different snapshot spaces that consist of harmonic functions in the oversampled region and dominant eigenmodes of a local spectral problem in the oversampled region. For the local spectral problems, we also consider various choices by considering mass and energy matrices in the oversampled regions. Our numerical results show that the proposed methods converge as we increase the dimension of the space and this convergence is consistent with our theoretical findings. We also test the use of multiple spectral problems in constructing basis functions as well as modifying the conductivity outside the target block to improve the accuracy.

The paper is organized in the following way. In the next section, Section 2, we present the problem setting and the definitions of coarse grids. In Section 3, we present the construction of local basis functions. Section 4 is devoted to the numerical results. In Section 5 we present the analysis of the method and in Section 6 we offer some concluding remarks.

2. Preliminaries

We consider elliptic equations of the form

$$- \operatorname{div}\big(\kappa(x;\mu)\,\nabla u\big) = f \text{ in } D, \tag{1}$$

where u is prescribed on ∂D and μ is a parameter. We assume that $\kappa(x;\mu) = \sum_{q=1}^{Q} \Theta(\mu_q)\kappa_q(x)$ and that the coefficient $\kappa(x;\cdot)$ has multiple scale and high variations (e.g., see Fig. 1 for $\kappa_1(x)$ and $\kappa_2(x)$ used in simulations).

To discretize (1), we next introduce the notion of fine and coarse grids. We let $\mathcal{T}^H$ be a usual conforming partition of the computational domain D into finite elements (triangles, quadrilaterals, tetrahedrals, etc.). We refer to this partition as the coarse grid and assume that each coarse subregion is partitioned into a connected union of fine grid blocks. The fine grid partition will be
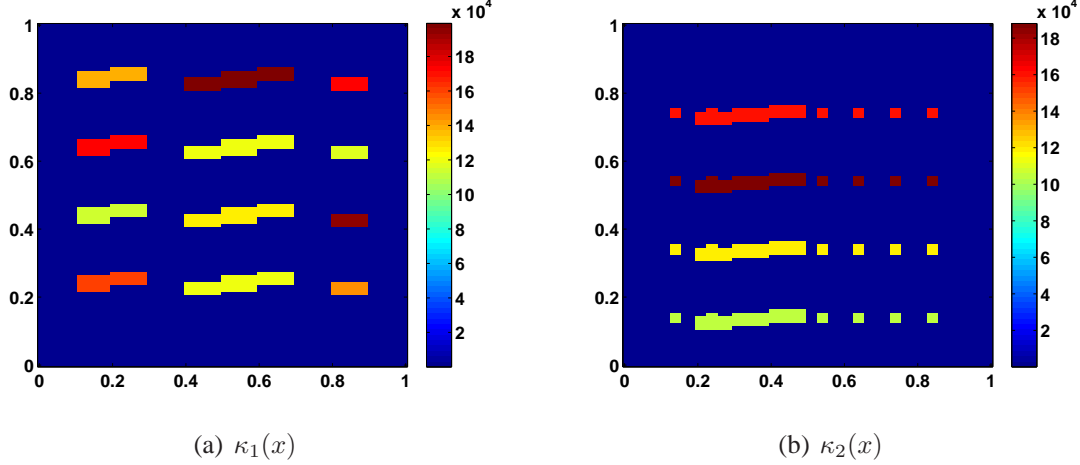
(a) $\kappa_1(x)$　　　　　　　　(b) $\kappa_2(x)$

Figure 1: Decomposition of permeability field

denoted by $\mathcal{T}^h$. We use $\{x_i\}_{i=1}^{N_v}$ (where N_v the number of coarse nodes) to denote the vertices of the coarse mesh $\mathcal{T}^H$, and define the neighborhood of the node x_i by

$$\omega_i = \bigcup\{K_j \in \mathcal{T}^H; \quad x_i \in \overline{K}_j\}. \tag{2}$$

See Fig. 2 for an illustration of neighborhoods and elements subordinated to the coarse discretization. Furthermore, we introduce a notation for an oversampled region. We denote by ω_i^+ an oversampled region of $\omega_i \subset \omega_i^+$. In general, we will consider oversampled regions ω_i^+ defined by adding several fine-grid or coarse-grid layers around ω_i.

Next, we briefly outline the global coupling and the role of coarse basis functions for the respective formulations that we consider. Throughout this paper, we use the continuous Galerkin formulation, and use ω_i as the support of basis functions even though ω_i^+ will be used in constructing multiscale basis functions. For the purpose of this description, we formally denote the basis functions of the online space V_{on} by $\psi_k^{\omega_i}$. The solution will be sought as $u_H(x; \mu) = \sum_{i,k} c_k^i \psi_k^{\omega_i}(x; \mu)$.

Once the basis functions are identified, the global coupling is given through the variational form

$$a(u_H, v; \mu) = (f, v), \quad \text{for all } v \in V_{\text{on}}, \tag{3}$$

and

$$a(u, v; \mu) = \int_D \kappa(x; \mu) \nabla u \nabla v.$$

We note that in the case when the coefficient is independent of the parameter, then $V_{\text{on}} = V_{\text{off}}$.

4

3. Local basis functions

In this section we describe the offline-online computational procedure, and elaborate on some applicable choices for the associated bilinear forms to be used in the coarse space construction. Below we offer a general outline for the procedure.

1. Offline computations:

   - 1.0. Coarse grid generation.
   - 1.1. Construction of snapshot space that will be used to compute an offline space.
   - 1.2. Construction of a small dimensional offline space by performing dimension reduction in the space of local snapshots.

2. Online computations:

   - 2.1. For each input parameter, compute multiscale basis functions.
   - 2.2. Solution of a coarse-grid problem for any force term and boundary condition.
   - 2.3. Iterative solvers, if needed.

In the offline computation, we first construct a snapshot space $V_{\text{snap}}^{\omega_i^+}$ or $V_{\text{snap}}^{\omega_i}$, depending on the choice of domain to generate the snapshot space, where ω_i^+ is an oversampled region that contains a coarse neighborhood ω_i. Construction of the snapshot space involves solving the local problems for various choices of input parameters, and we describe the details below.

3.1. Snapshot space

3.1.1. Harmonic extensions in oversampled region

Our first choice of snapshot space consists of harmonic extension of fine-grid functions defined on the boundary of ω_i^+. More precisely, for each fine-grid function, $\delta_l^h(x)$, which is defined by $\delta_l^h(x) = \delta_{l,k}$, $\forall l, k \in J_h(\omega_i^+)$, where $J_h(\omega_i^+)$ denotes the fine-grid boundary node on $\partial \omega_i^+$.

For parameter-independent problem, we solve

$$-div(\kappa(x)\nabla \psi_l^{+,\text{snap}}) = 0 \ \text{ in } \omega_i^+$$

subject to boundary condition, $\psi_l^{+,\text{snap}} = \delta_l^h(x)$ on $\partial \omega_i^+$.

For parameter-dependent one, we can choose several values μ_j, $j = 1, \ldots, J$ (J denotes the number of parameters used) to generate the snapshot space separately as above and combine them to obtain the snapshot space (see details in Section 4.2).
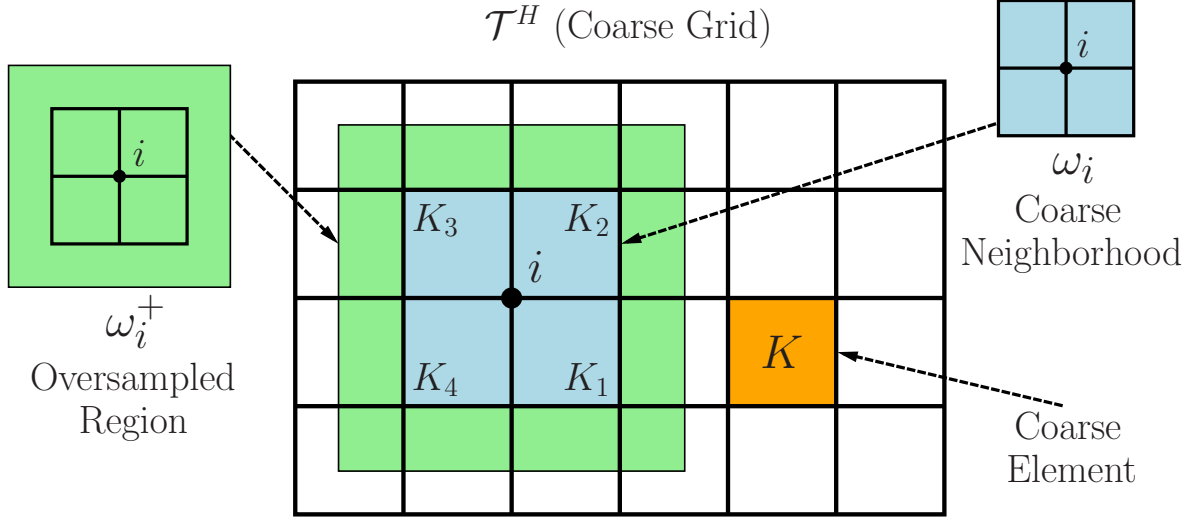
Figure 2: Illustration of a coarse neighborhood and oversampled domain

3.1.2. Local spectral basis in oversampled region

We propose to solve the following zero Neumann eigenvalue problem on an oversampled domain ω_i^+:

$$A^+(\mu_j)\psi_{l,j}^{+,\text{snap}} = \lambda_{l,j}^{+,\text{snap}}S^+(\mu_j)\psi_{l,j}^{+,\text{snap}} \text{ in } \omega_i^+, \tag{4}$$

where μ_j $(j = 1, \ldots, J)$ is a specified set of fixed parameter values, and we emphasize that the superscript $+$ signifies that the eigenvalue problem is solved in an oversampled coarse subdomain ω_i^+. The matrices in Eq. (4) are defined as

$$A^+(\mu_j) = [a^+(\mu_j)_{mn}] = \int_{\omega_i^+} \kappa(x; \mu_j)\nabla\phi_n\cdot\nabla\phi_m \quad \text{and} \quad S^+(\mu_j) = [s^+(\mu_j)_{mn}] = \int_{\omega_i^+} \widetilde{\kappa}(x; \mu_j)\phi_n\phi_m, \tag{5}$$

where ϕ_n denotes the standard bilinear, fine-scale basis functions and the form for $\widetilde{\kappa}$ will be discussed in Section 5. In our numerical implementations, we take $\widetilde{\kappa} = \kappa$, though one can use multiscale basis functions, χ_i^+ in ω_i^+, to construct $\widetilde{\kappa}$ as $\widetilde{\kappa} = \sum_i \kappa|\nabla\chi_i^+|^2$ (see [13, 18] for more discussions on the choice of partition of unity functions). We note that Eq. (4) is the discretized form of the continuous equation

$$-\text{div}(\kappa(x; \mu_j)\nabla\psi_{l,j}^{+,\text{snap}}) = \lambda_{l,j}^{+,\text{snap}}\widetilde{\kappa}(x; \mu_j)\psi_{l,j}^{+,\text{snap}} \quad \text{in } \omega_i^+.$$

After solving Eq. (4), we keep the first L_i eigenfunctions corresponding to the dominant eigen-

values (asymptotically vanishing in this case) to form the space

$$V_{\text{snap}}^+ = \text{span}\{\psi_{l,j}^{+,\text{snap}} : \quad 1 \le j \le J \text{ and } 1 \le l \le L_i\},$$

for each oversampled coarse neighborhood ω_i^+. We note that in the case when ω_i is adjacent to the global boundary, no oversampled domain is used. For the sake of simplicity, throughout, we denote continuous and discrete solutions by the same symbol (e.g., $\psi_{l,j}^{+,\text{snap}}$ in the above case).

We reorder the snapshot functions using a single index to create the matrices

$$R_{\text{snap}}^+ = \left[\psi_1^{+,\text{snap}}, \ldots, \psi_{M_{\text{snap}}}^{+,\text{snap}}\right] \quad \text{and} \quad R_{\text{snap}} = \left[\psi_1^{\text{snap}}, \ldots, \psi_{M_{\text{snap}}}^{\text{snap}}\right],$$

where ψ_j^{snap} denotes the restriction of $\psi_j^{+,\text{snap}}$ to ω_i, and M_{snap} denotes the total number of functions to keep in the snapshot matrix construction.

Note that the above process to generate local spectral basis is also applied to parameter-independent problems.

3.2. Offline space

We will discuss two types of offline spaces where the first one will use one spectral problem in the snapshot space and the other one will use multiple spectral problems in the snapshot space (following Theorem 3.3 of [4]).

3.2.1. Offline space using a single spectral problem

In order to construct an oversampled offline space V_{off}^+ or standard neighborhood offline space V_{off}, we perform a dimension reduction in the space of snapshots using an auxiliary spectral decomposition. The main objective is to use the offline space to efficiently (and accurately) construct a set of multiscale basis functions for each μ value in the online stage. More precisely, we seek a subspace of the snapshot space such that it can approximate any element of the snapshot space in the appropriate sense defined via auxiliary bilinear forms. At the offline stage the bilinear forms are chosen to be *parameter-independent*, such that there is no need to reconstruct the offline space for each μ value. We will consider the following eigenvalue problems in the space of snapshots:

$$A^{\text{off}} \Psi_k^{\text{off}} = \lambda_k^{\text{off}} S^{\text{off}} \Psi_k^{\text{off}} \tag{6}$$

or

$$A^{+,\text{off}} \Psi_k^{\text{off}} = \lambda_k^{\text{off}} A^{\text{off}} \Psi_k^{\text{off}} \tag{7}$$

or

$$A^{\text{off}} \Psi_k^{\text{off}} = \lambda_k^{\text{off}} S^{+,\text{off}} \Psi_k^{\text{off}} \tag{8}$$

or

$$A^{+,\text{off}} \Psi_k^{\text{off}} = \lambda_k^{\text{off}} S^{+,\text{off}} \Psi_k^{\text{off}} \tag{9}$$

where

$$A^{\text{off}} = [a_{mn}^{\text{off}}] = \int_{\omega_i} \overline{\kappa}(x; \mu) \nabla \psi_m^{\text{snap}} \cdot \nabla \psi_n^{\text{snap}} = R_{\text{snap}}^T \overline{A} R_{\text{snap}},$$

$$S^{\text{off}} = [s_{mn}^{\text{off}}] = \int_{\omega_i} \widetilde{\overline{\kappa}}(x; \mu) \psi_m^{\text{snap}} \psi_n^{\text{snap}} = R_{\text{snap}}^T \overline{S} R_{\text{snap}},$$

$$A^{+,\text{off}} = [a_{mn}^{+,\text{off}}] = \int_{\omega_i^+} \overline{\kappa}(x, \mu) \nabla \psi_m^{+,\text{snap}} \cdot \nabla \psi_n^{+,\text{snap}} = \left(R_{\text{snap}}^+\right)^T \overline{A}^+ R_{\text{snap}}^+,$$

$$S^{+,\text{off}} = [s_{mn}^{+,\text{off}}] = \int_{\omega_i^+} \widetilde{\overline{\kappa}}(x, \mu) \psi_m^{+,\text{snap}} \psi_n^{+,\text{snap}} = \left(R_{\text{snap}}^+\right)^T \overline{S}^+ R_{\text{snap}}^+.$$

The coefficients $\overline{\kappa}(x, \mu)$ and $\widetilde{\overline{\kappa}}(x, \mu)$ are parameter-averaged coefficients (see [12]). Again, we will take $\widetilde{\overline{\kappa}}(x, \mu) = \overline{\kappa}(x, \mu)$ though one can use multiscale partition of unity functions to compute $\widetilde{\overline{\kappa}}(x, \mu)$ (cf. [13]). We note that $\overline{A}^+$ and $\overline{A}$ denote analogous fine scale matrices as defined in Eq. (4), except that parameter-averaged coefficients are used in the construction, and that A is constructed by integrating only on ω_i. To generate the offline space we then choose the smallest M_{off} eigenvalues from one of Eqs. (6)-(8) and form the corresponding eigenvectors in the respective space of snapshots by setting $\psi_k^{+,\text{off}} = \sum_j \Psi_{kj}^{\text{off}} \psi_j^{+,\text{snap}}$ or $\psi_k^{\text{off}} = \sum_j \Psi_{kj}^{\text{off}} \psi_j^{\text{snap}}$ (for $k = 1, \ldots, M_{\text{off}}$), where Ψ_{kj}^{off} are the coordinates of the vector Ψ_k^{off}. We then create the offline matrices

$$R_{\text{off}}^+ = \left[\psi_1^{+,\text{off}}, \ldots, \psi_{M_{\text{off}}}^{+,\text{off}}\right] \quad \text{and} \quad R_{\text{off}} = \left[\psi_1^{\text{off}}, \ldots, \psi_{M_{\text{off}}}^{\text{off}}\right]$$

to be used in the online space construction.

Remark 1. *At this stage, we note that in the case when we have a parameter-independent coefficient in Eq. (1), many of the expressions in this section are simplified. In particular, there is no need*

for averaging the coefficients in order to create the respective (offline) mass and (offline) stiffness matrices. Furthermore, the offline space represents the final space in which the enriched multiscale solutions will be computed. Thus, the discussion of online space creation below is limited to the case when the problem is parameter-dependent.

Remark 2. *Our analysis in Section 5 shows that the convergence of the GMsFEM is proportional to the reciprocal of the eigenvalue that the corresponding eigenvector is not included in the coarse space. We have compared the decay of the reciprocal of eigenvalues for Eq. (6), Eq. (7), and Eq. (8) (by choosing a subdomain for $\kappa(x)$ in Fig. 4). We plot the decay of the eigenvalues for a coarse block in Fig. 3 (note logarithmic y-scale). As we observe from this figure that the decay of eigenvalues corresponding to Eq. (8) (when oversampling is used in formulating the eigenvalue problem) is faster compared to Eq. (6) (when no oversampling is used).*

### 3.2.2. Offline space using multiple spectral problems

Motivated by Theorem 3.3 of [4], we propose an offline space that uses both Eq. (6) and Eq. (9). In particular, using dominant eigenvectors of both Eq. (6) and Eq. (9), we take a union of these eigenvectors to construct an offline space. In particular, as described above, we use $\psi_k^{+,\mathrm{off}} = \sum_j \Psi_{kj}^{+,\mathrm{off}} \psi_j^{+,\mathrm{snap}}$ (for $k = 1, \dots, M_{+,\mathrm{off}}$) or $\psi_k^{\mathrm{off}} = \sum_j \Psi_{kj}^{\mathrm{off}} \psi_j^{\mathrm{snap}}$ (for $k = 1, \dots, M_{\mathrm{off}}$), where $\Psi_{kj}^{+,\mathrm{off}}$ are the coordinates of the vector Ψ_k^{off} in Eq. (9) and Ψ_{kj}^{off} are the coordinates of the vector Ψ_k^{off} in Eq. (6). Then, the offline space is constructed as a union of ψ_k^{off} and $\psi_k^{+,\mathrm{off}}$ after eliminating linearly dependent vectors. We present an analysis in Section 5.2 and numerical results in Section 4.1.1.

### 3.3. Online space for parameter-dependent case

We only describe the online space using a single spectral problem. One can analogously construct the online space using multiple spectral problems. For the parameter-dependent case, we next construct the associated online coarse space $V_{\mathrm{on}}(\mu)$ *for each fixed μ* value on each coarse subdomain. In principle, we want this to be a small dimensional subspace of the offline space for computational efficiency. The online coarse space will be used within the finite element framework to solve the original global problem, where a continuous Galerkin coupling of the multiscale basis functions is used to compute the global solution. In particular, we seek a subspace of the respective offline space such that it can approximate any element of the offline space in an appropriate sense. We note that at the online stage, the bilinear forms are chosen to be *parameter-dependent*. Similar
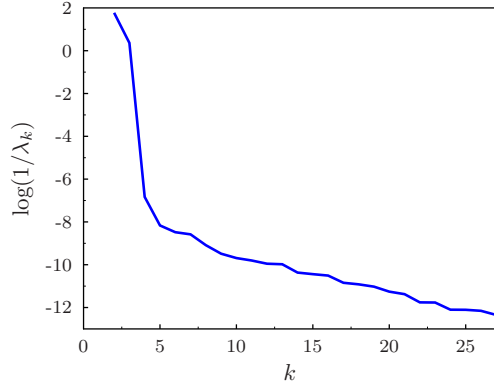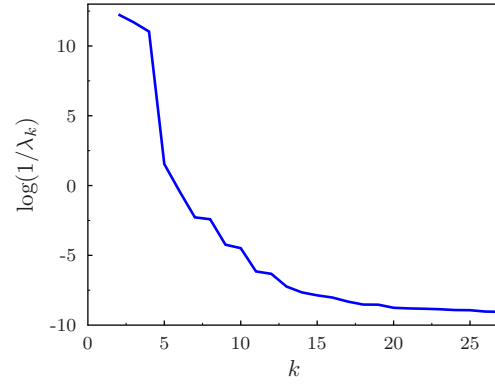
(a) Eigenvalue problem Eq. (6) with Harmonic snapshots
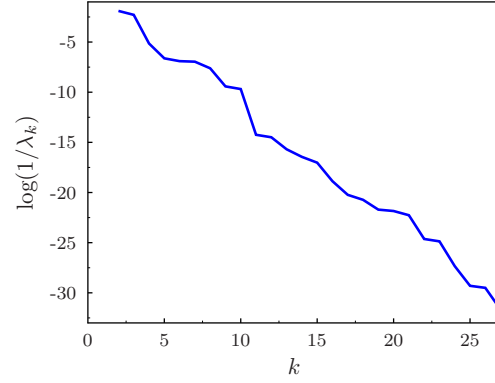
(b) Eigenvalue problem Eq. (7) with Harmonic snapshots
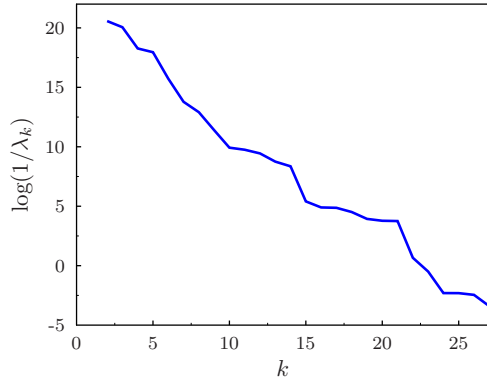
(c) Eigenvalue problem Eq. (8) with Harmonic snapshots

(d) Eigenvalue problem Eq. (8) with spectral snapshots

Figure 3: Eigenvalue decay on log-scale against the number of eigenvalues. x-axis indicates the number of eigenvalue and y-axis indicates the inverse of the eigenvalue (on log-scale)

analysis motivates the following eigenvalue problems posed in the offline space:

$$A^{\text{on}}(\mu)\Psi_k^{\text{on}} = \lambda_k^{\text{on}}S^{\text{on}}(\mu)\Psi_k^{\text{on}} \tag{10}$$

or

$$A^{+,\text{on}}(\mu)\Psi_k^{\text{on}} = \lambda_k^{\text{on}}A^{\text{on}}(\mu)\Psi_k^{\text{on}} \tag{11}$$

or

$$A^{\text{on}}(\mu)\Psi_k^{\text{on}} = \lambda_k^{\text{on}}S^{+,\text{on}}(\mu)\Psi_k^{\text{on}} \tag{12}$$

where

$$A^{\text{on}}(\mu) = [a^{\text{on}}(\mu)_{mn}] = \int_{\omega_i}\kappa(x;\mu)\nabla\psi_m^{\text{off}}\cdot\nabla\psi_n^{\text{off}} = R_{\text{off}}^T A(\mu)R_{\text{off}},$$

$$S^{\text{on}}(\mu) = [s^{\text{on}}(\mu)_{mn}] = \int_{\omega_i}\widetilde{\kappa}(x;\mu)\psi_m^{\text{off}}\psi_n^{\text{off}} = R_{\text{off}}^T S(\mu)R_{\text{off}},$$

$$A^{+,\text{on}}(\mu) = [a_{mn}^{+,\text{on}}(\mu)] = \int_{\omega_i^+}\kappa(x,\mu)\nabla\psi_m^{+,\text{off}}\cdot\nabla\psi_n^{+,\text{off}} = \left(R_{\text{off}}^+\right)^T A^+(\mu)R_{\text{off}}^+,$$

$$S^{+,\text{on}}(\mu) = [s_{mn}^{+,\text{on}}(\mu)] = \int_{\omega_i^+}\widetilde{\kappa}(x,\mu)\psi_m^{+,\text{off}}\psi_n^{+,\text{off}} = \left(R_{\text{off}}^+\right)^T S^+(\mu)R_{\text{off}}^+,$$

and $\kappa(x;\mu)$ and $\widetilde{\kappa}(x;\mu)$ are now parameter dependent. Again, we will take $\widetilde{\kappa}(x,\mu) = \kappa(x,\mu)$ in our simulations though one can use multiscale partition of unity functions to compute $\widetilde{\kappa}(x,\mu)$ (cf. [13]). To generate the online space we then choose the smallest M_{on} eigenvalues from one of Eqs. (10)-(12) and form the corresponding eigenvectors in the offline space by setting $\psi_k^{\text{on}} = \sum_j \Psi_{kj}^{\text{on}}\psi_j^{\text{off}}$ (for $k = 1, \ldots, M_{\text{on}}$), where Ψ_{kj}^{on} are the coordinates of the vector Ψ_k^{on}.

4. Numerical Examples

4.1. Parameter-independent case

First, we consider parameter-independent case

$$\kappa(x;\mu) = \kappa(x)$$

by choosing $\mu_1, \mu_2 = 0.5$ (see Fig. 4 for an illustration of the resulting permeability). In previous works, e.g., [13], $\widetilde{\kappa}$ takes the general form $\widetilde{\kappa} = \kappa \sum_i H^2|\nabla\chi_i|^2$, where χ_i denotes an original partition of unity [12], although we take $\widetilde{\kappa} = \kappa$ for the majority of examples in this section. The fine-grid is chosen to be 100×100. We consider two coarse grids, 10×10 and 20×20. The error
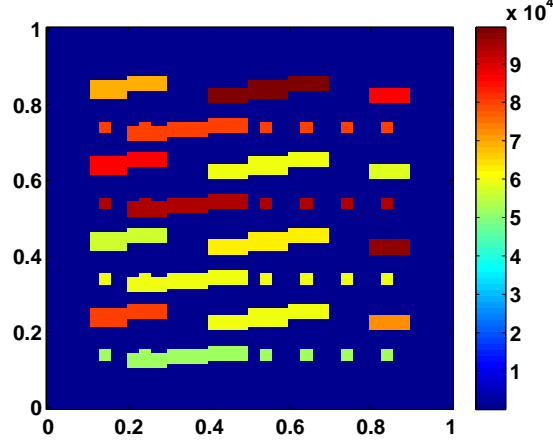
11

Figure 4: Permeability field used in Section 4.1

will be measured in weighted L^2 and weighted H^1 norms defined as

$$\|u\|_{L^2_\kappa} = \left(\int_D \kappa u^2 \right)^{\frac{1}{2}}, \quad \|u\|_{H^1_\kappa} = \left(\int_D \kappa |\nabla u|^2 \right)^{\frac{1}{2}}.$$

Then Eq. (1) is solved with $f = 1$ and linear Dirichlet boundary condition.

In the first set of numerical examples, 10×10 coarse grid and the oversampling region of the size of 10 fine-grid blocks in each direction is chosen (i.e., the oversampled region contains an extra coarse block layer around ω_i). We denote this oversampled region by $\omega_i^+ = 3 \times \omega_i$. We use the eigenvalue problems Eq. (6), Eq. (7), and Eq. (8) in the space of snapshots generated in the oversampled region by harmonic extensions as in Subsection 3.1.1. In all numerical cases, we take $\widetilde{\kappa} = \kappa$. In Tables 1, 2, and 3, we present the errors for weighted L^2 norm and weighted H^1 norm. As we observe that all cases predict similar convergence errors that decrease as we increase the dimension of the space. We note that in this case there is a residual error because of the fact that we use harmonic functions as a space of snapshots and thus we can not approximate the error due to the source term. This error for 10×10 coarse mesh is about 10% (or order of coarse mesh size). Because of this irreducible error, the convergence of GMsFEM deteriorates and remains at 10%.

In the next example, we consider a smaller oversampled region that includes only one fine grid block. We denote this by $\omega_i^+ = \omega_i + 1$. We have tested various oversampled region sizes and include only one representative example. In this example (see results in Table 4), we observe similar error behavior as those in previous examples.

As we discussed earlier, the error between the fine scale solution and GMsFEM solution contains an irreducible error because of the fact that the harmonic snapshots are used and these snap-

dim(V_{off})	Λ_*	$\|u - u^{\mathrm{off}}\|$ (%)	
		$L^2_\kappa(D)$	$H^1_\kappa(D)$
364	1.04×10^3	0.46	17.26
526	2.62×10^3	0.42	13.84
688	4.29×10^3	0.33	11.92
909	1.15×10^5	0.30	10.90

Table 1: Relative errors between the fine scale solution and **offline spaces**; Eigenvalue problem from Eq. (6), 10×10 coarse mesh, harmonic snapshots, $\omega_i^+ = 3 \times \omega_i$.

dim(V^+_{off})	Λ_*	$\|u - u^{+,\mathrm{off}}\|$ (%)	
		$L^2_\kappa(D)$	$H^1_\kappa(D)$
364	33.16	4.22	33.69
526	105.32	0.65	16.59
688	669.50	0.32	11.95
909	8.12×10^6	0.30	10.82

Table 2: Relative errors between the fine scale solution and **offline spaces**; Eigenvalue problem from Eq. (7), 10×10 coarse mesh, harmonic snapshots, $\omega_i^+ = 3 \times \omega_i$.

shots can not approximate the effects of the right hand side. This error can be easily estimated for high-contrast problems considered in this paper and it is of order $O(H)$. First, we consider the use of dominant eigenvectors as a space of snapshots that correspond to smallest eigenvalues of Eq. (6) in $\omega_i^+ = 3 \times \omega_i$ as a snapshot space. In this snapshot space, we apply Eq. (8) and identify dominant modes in the target domain as before. The numerical results are presented in Table 5. As we observe from these results that the error is smaller when eigenvector snapshots are used. In general, when comparing to the fine-scale solution, one can also use fewer modes corresponding to the space of harmonic snapshots and some extra modes that represent source term within the local domain (e.g., modes that correspond to homogeneous Dirichlet eigenvalue problem). In Table 6, we present numerical results, where the GMsFEM solution is compared to the solution computed in the space of harmonic snapshots. In this setup, there is no irreducible error and the method

dim(V^+_{off})	Λ_*	$\|u - u^{+,\mathrm{off}}\|$ (%)	
		$L^2_\kappa(D)$	$H^1_\kappa(D)$
364	2.11×10^{-4}	4.47	45.99
526	8.62×10^{-4}	1.62	27.65
688	0.0018	0.28	14.54
909	0.0093	0.30	11.09

Table 3: Relative errors between the fine scale solution and **offline spaces**; Eigenvalue problem from Eq. (8), 10×10 coarse mesh, harmonic snapshots, $\omega_i^+ = 3 \times \omega_i$.

$\dim(V_{\text{off}}^+)$	Λ_*	$\|u - u^{+,\text{off}}\|$ (%)	
		$L_\kappa^2(D)$	$H_\kappa^1(D)$
526	0.03	1.64	25.51
850	0.08	0.38	14.82
2470	533.50	0.31	12.10
3280	1.08×10^3	0.30	11.42

Table 4: Relative errors between the fine scale solution and **offline spaces**; Eigenvalue problem from Eq. (8), 10×10 coarse mesh, harmonic snapshots, $\omega_i^+ = \omega_i + 1$.

converges to the fine scale solution. Moreover, we notice that the errors are smaller.

$\dim(V_{\text{off}}^+)$	Λ_*	$\|u - u^{+,\text{off}}\|$ (%)	
		$L_\kappa^2(D)$	$H_\kappa^1(D)$
364	0.0045	0.27	17.49
688	0.055	0.08	9.88
1012	0.91	0.07	7.33
1660	37.3	0.03	4.04
3280	1.68×10^3	0.004	1.10

Table 5: Relative errors between the fine scale solution and **offline spaces**; Eigenvalue problem from Eq. (8), 10×10 coarse mesh, eigenvalue snapshots, $\omega_i^+ = 3 \times \omega_i$.

$\dim(V_{\text{off}}^+)$	Λ_*	$\|u^{+,909} - u^{+,\text{off}}\|$ (%)	
		$L_\kappa^2(D)$	$H_\kappa^1(D)$
364	2.11×10^{-4}	4.69	44.36
526	8.62×10^{-4}	1.75	25.17
688	0.0018	0.16	9.34
860	0.0070	0.05	3.85

Table 6: Relative errors between the maximal dimension offline solution ($u^{+,909}$) and **offline spaces** obtained from using oversampled domains; Eigenvalue problem from Eq. (8), 10×10 coarse mesh, harmonic snapshots, $\omega_i^+ = 3 \times \omega_i$.

For the next set of numerical examples, we use 20×20 coarse-grid. In Table 7, we present numerical results when the eigenvalue problem Eq. (8) is used. As in the case of 10×10 coarse grid, there is an irreducible error; however, it is lower (about 5%), because of the coarse mesh size. To remove the irreducible error, we compare the GMsFEM solution to the solution computed with snapshot vectors in Table 8. As we observe that the error is smaller and it will converge to zero as we increase the dimension of the coarse space. We also present an error when a different oversampling domain size is used in Table 9. The results are not sensitive to the oversampling domain size as these results show. In Table 10, we present relative errors when the snapshot space

is chosen to consist of eigenvectors as defined in Eq. 4 (cf. Table 5). In this case, similar to Table 5, we observe smaller errors when the snapshot space consists of eigenvectors in Eq. 4. We also present a numerical result in Table 11 where the coefficients in $\omega_i^+ \backslash \omega_i$ reduced by $1e+4$ to diminish the constant in the estimates presented in Section 5.1.

$\dim(V_{\text{off}}^+)$	Λ_*	$\|u - u^{+,\text{off}}\|$ (%)	
		$L_\kappa^2(D)$	$H_\kappa^1(D)$
1524	3.25×10^{-5}	2.69	36.37
2168	1.70×10^{-4}	0.65	18.42
2705	4.71×10^{-4}	0.21	11.04
3471	0.014	0.07	5.03

Table 7: Relative errors between the fine scale solution and **offline spaces** obtained from using oversampled domains; Eigenvalue problem from Eq. (8), 20×20 coarse mesh, harmonic snapshots, $\omega_i^+ = 3 \times \omega_i$.

$\dim(V_{\text{off}}^+)$	Λ_*	$\|u^{+,3471} - u^{+,\text{off}}\|$ (%)	
		$L_\kappa^2(D)$	$H_\kappa^1(D)$
1524	3.25×10^{-5}	2.72	35.98
2168	1.70×10^{-4}	0.69	17.70
2705	4.71×10^{-4}	0.22	9.82
3182	0.0059	0.02	3.21

Table 8: Relative errors between the maximal dimension offline solution ($u^{+,3471}$) and **offline spaces** obtained from using oversampled domains; Eigenvalue problem from Eq. (8), 20×20 coarse mesh, harmonic snapshots, $\omega_i^+ = 3 \times \omega_i$.

$\dim(V_{\text{off}})$	Λ_*	$\|u - u^{\text{off}}\|$ (%)	
		$L_\kappa^2(D)$	$H_\kappa^1(D)$
1524	0.03	0.27	19.47
2607	0.06	0.15	12.39
3690	0.16	0.07	9.40
7300	684.14	0.05	3.70

Table 9: Relative errors between the fine scale solution and **offline spaces** obtained from using oversampled domains; Eigenvalue problem from Eq. (8), 20×20 coarse mesh, harmonic snapshots, $\omega_i^+ = \omega_i + 1$.

Finally, we plot the energy error against $(1/\Lambda_*)^{\frac{1}{2}}$ for 10×10 and 20×20 cases in Figs. 5. The correlation between the errors and $1/\Lambda_*$ is over 0.93 when we consider 10×10 mesh case (as in Figs. 5(a) and 5(c)). In Figs. 5(b) and 5(d), we depict the relative errors corresponding to Tables 8 and 10. In this case, we also observe a good agreement and the correlation to be over 0.98.

15

| $\dim(V_{\text{off}}^+)$	Λ_*	$\|u - u^{+,\text{off}}\|$ (%)	
		$L_\kappa^2(D)$	$H_\kappa^1(D)$
1524	0.002	1.25	28.54
2102	0.009	0.22	14.34
2607	0.014	0.12	8.25
3596	1.03×10^3	0.01	2.06

Table 10: Relative errors between the fine scale solution and **offline spaces** obtained from using oversampled domains; Eigenvalue problem from Eq. (8), 20×20 coarse mesh, eigenvalue snapshots, $\omega_i^+ = 3 \times \omega_i$.

| $\dim(V_{\text{off}}^+)$	Λ_*	$\|u - u^{+,\text{off}}\|$ (%)	
		$L_\kappa^2(D)$	$H_\kappa^1(D)$
1524	0.23	0.75	21.01
2168	0.82	0.18	13.19
2705	2.45	0.08	8.67
3471	117.18	0.07	4.44

Table 11: Relative errors between the fine scale solution and **offline spaces** obtained from using oversampled domains with $\kappa = \frac{\kappa}{10^4}$ in $\omega_i^+\backslash\omega_i$; Eigenvalue problem from Eq. (8), 20×20 coarse mesh, harmonic snapshots, $\omega_i^+ = 3 \times \omega_i$.

### 4.1.1. Parameter-independent case using multiple spectral problems

In this section, we study the use of multiple spectral problems as described in Section 3.2.2. In particular, we use only two spectral problems in ω and ω^+. The results are presented in Tables 12 and 13. As the convergence theory indicates, for the same eigenvalue threshold, one can expect the quadratic decay in the convergence rate with a constant that is described in Section 5.2. In Table 12, we compare the offline solution and the fine grid solution, while in Table 13, we compare the offline solution and the snapshot solution. In both cases, we observe that the square of the error resulting from a single spectral problem correlates well to the case corresponding to multiple spectral problems. This behavior deteriorates when the space dimension is large due to irreducible error. For this set of numerical results, we observe that the coarse space dimension resulting from multiple spectral problems is large compared to the case when a single spectral problem is used. However, we note that our convergence result does not contain any information about the dimension of the coarse space, but only about an eigenvalue threshold. On the other hand, our convergence analysis suggests that the coarse space needs to include an approximation in both ω and ω^+. The eigenvectors of Eq. (9) may be represented using the eigenvectors of Eq. (6), and thus one can use the respective eigenvectors to complement each other. Our numerical results show that by combining eigenvectors of Eq. (6) and Eq. (9), one can achieve better convergence compared to only using Eq. (6) in our pre-asymptotic numerical simulations.
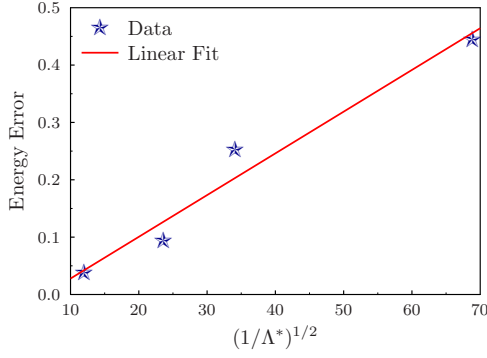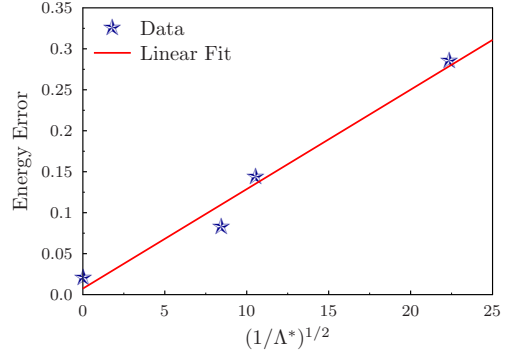
(a) $N = 10$, corrcoef=0.98
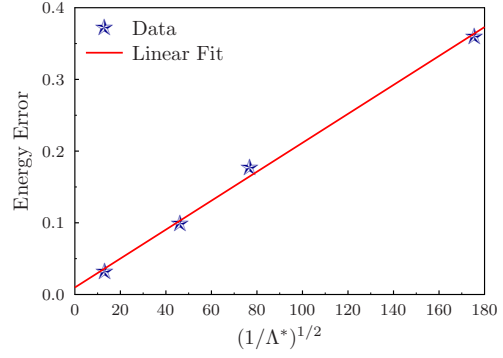
(b) $N = 20$, corrcoef=0.99
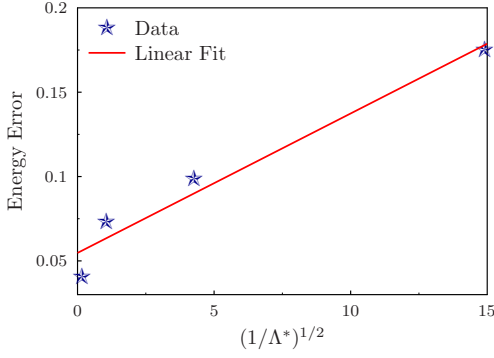
(c) $N = 10$, corrcoef=0.93, eigenvalue snaps

(d) $N = 20$, corrcoef=0.97, eigenvalue snaps

Figure 5: Relation between relative energy error and Λ_* for Tables 6, 8, 5 and 10 respectively.

4.2. Parameter-dependent case

For the next set of numerical results, we consider a parameter-dependent example where

$$\kappa(x; \mu) = \mu_1 \kappa_1(x) + \mu_2 \kappa_2(x),$$

where $\kappa_1(x)$ and $\kappa_2(x)$ are depicted in Fig. 1. For the numerical examples, we consider a snapshot space that consists of solving local eigenvalue problem described by Eq. (6) in $\omega_i^+ = 3 \times \omega_i$ for 9 selected values of $\mu = (\mu_1, \mu_2)$. By choosing 20 dominant eigenvectors for each of 9 selected values of μ and ensuring linear independence, we form the space of snapshots. In this space of snapshots, we use the operator averaged over μ to construct the offline space. In particular, we consider 3 choices for offline eigenvalue problems that are given by Eq. (6), Eq. (7), and Eq. (8). These local eigenvalue problems are used to construct the offline space. Furthermore, we use the same eigenvalue problems for an online value of the parameter, to construct an online space which

$\dim(V_{\text{off}})$	Λ^*	$H^1_\kappa(D)$ (%) (Eqs. (9), (6))	$H^1_\kappa(D)$ (%) (Eq. (6))
791(618)	60.52(147.82) (tol = 60(100))	31.47	38.34
1172(733)	401.56(1.01×10^3) (tol = 400(1000))	14.72	24.42
2054(1568)	1.00(5.05)$\times10^3$ (tol = 1000(5000))	8.28	10.73

Table 12: Relative errors between the fine scale solution and **offline spaces** for local spectral problems using a single (Eq. (6)) and multiple eigenvalue problems (Eq. (9) and (6)). 20×20 coarse mesh, harmonic snapshots, $\omega_i^+ = 3 \times \omega_i$.

$\dim(V_{\text{off}})$	Λ^*	$H^1_\kappa(D)$ (%) (Eqs. (9), (6))	$H^1_\kappa(D)$ (%) (Eq. (6))
791(618)	60.52(147.82) (tol = 60(100))	31.26	38.16
1172(733)	401.56(1.01×10^3) (tol = 400(1000))	14.31	24.16
2054(1568)	1.00(5.05)$\times10^3$ (tol = 1000(5000))	7.53	10.16

Table 13: Relative errors between the snapshot solution and **offline spaces** for local spectral problems using a single (Eq. (6)) and multiple eigenvalue problems (Eq. (9) and (6)). 20×20 coarse mesh, harmonic snapshots, $\omega_i^+ = 3 \times \omega_i$.

is a subspace of the offline space by solving the local eigenvalue problem Eq. (10), Eq. (11), and Eq. (12). The results are presented in Tables 14, 15, 16, respectively. We see from these results that the GMsFEM converges in all the cases considered above. The best convergence among the three choices it found in Table 16.

$\dim(V_{\text{on}})$	Λ_*	$\|u - u^{\text{on}}\|$ (%)		$\|u^{\text{on}} - u^{\text{off}}\|$ (%)	
		$L^2_\kappa(D)$	$H^1_\kappa(D)$	$L^2_\kappa(D)$	$H^1_\kappa(D)$
728	537.1	0.26	11.20	0.18	9.50
907	1.05×10^3	0.18	8.62	0.09	6.27
1037	1.93×10^3	0.17	8.22	0.09	5.72
1248	3.22×10^3	0.11	6.42	0.02	2.55
1378	—	0.10	5.89	0.00	0.00

Table 14: Relative errors between the fine scale solution (and offline) and **online spaces** obtained from using non-oversampled domains; Eigenvalue problem from Eq. (10), 10×10 coarse mesh, eigenvalue snapshots, $\omega_i^+ = 3 \times \omega_i$.

5. Convergence studies and discussions. Parameter-independent case

5.1. Offline space using a single spectral problem

We define $I^{\omega_i}u$ and $I^{\omega_i^+}u$ as an interpolation of u in ω_i and ω_i^+ that will be chosen. Because the snapshot functions are defined in ω_i^+, $I^{\omega_i}u = I^{\omega_i^+}u$ in ω_i. We have

$$-\text{div}(\kappa(x)\nabla(u - I^{\omega_i}u)) = g \text{ in } \omega_i,$$
$$-\text{div}(\kappa(x)\nabla(u - I^{\omega_i^+}u)) = g \text{ in } \omega_i^+, \tag{13}$$

dim(V_{on}^+)	Λ_*	$\|u - u^{+,on}\|$ (%)		$\|u^{+,on} - u^{+,off}\|$ (%)	
		$L_\kappa^2(D)$	$H_\kappa^1(D)$	$L_\kappa^2(D)$	$H_\kappa^1(D)$
826	11.47	0.27	10.93	0.18	9.19
988	40.84	0.17	8.37	0.09	5.93
1133	65.10	0.10	6.23	0.01	2.02
1280	350.0	0.10	6.03	0.007	1.27
1378	—	0.10	5.89	0.00	0.00

Table 15: Relative errors between the fine scale (and offline) solution and **online spaces** obtained from using oversampled domains; Eigenvalue problem from Eq. (11), 10×10 coarse mesh, eigenvalue snapshots, $\omega_i^+ = 3 \times \omega_i$.

dim(V_{on}^+)	Λ_*	$\|u - u^{+,on}\|$ (%)		$\|u^{+,on} - u^{+,off}\|$ (%)	
		$L_\kappa^2(D)$	$H_\kappa^1(D)$	$L_\kappa^2(D)$	$H_\kappa^1(D)$
790	4.33×10^{-4}	0.22	10.37	0.25	8.51
888	0.0032	0.09	7.90	0.06	5.25
1133	3.27	0.10	6.29	0.03	2.18
1280	154.3	0.10	5.96	0.004	0.87
1378	—	0.10	5.89	0.00	0.00

Table 16: Relative errors between the fine scale (and offline) solution and **online spaces** obtained from using oversampled domains; Eigenvalue problem from Eq. (12), 10×10 coarse mesh, eigenvalue snapshots, $\omega_i^+ = 3 \times \omega_i$.

where g is the source term, $g = f + \mathrm{div}(\kappa(x)\nabla I^{\omega_i}u)$. Furthermore, we define χ_i and χ_i^+ as partition of unity functions subordinated to ω_i and ω_i^+. In particular, we can assume that χ_i and χ_i^+ are standard bilinear partition of unity functions for a rectangular partition. In general, we do not require χ_i^+ to be a partition of unity function; however, we require χ_i^+ to be zero on $\partial\omega_i^+$ and

$$|\nabla\chi_i|^2 \preceq |\nabla\chi_i^+|^2.$$

This is satisfied for bilinear functions.

Multiplying both sides of (13) by $\chi_i^2(u - I^{\omega_i}u)$ (or $(\chi_i^+)^2(u - I^{\omega_i^+}u)$ for the equation in ω_i^+), integrating by parts and re-arranging the terms, we have

$$\int_{\omega_i} \kappa\chi_i^2|\nabla(u - I^{\omega_i}u)|^2$$
$$\leq \frac{1}{C}\int_{\omega_i}\kappa|\nabla\chi_i|^2|(u - I^{\omega_i}u)|^2 + C\int_{\omega_i}\kappa\chi_i^2|\nabla(u - I^{\omega_i}u)|^2 + |\int_{\omega_i}g\chi_i^2(u - I^{\omega_i}u)|,$$

19

where $C < 1$ is independent of contrast. From here, we get

$$\int_{\omega_i} \kappa \chi_i^2 |\nabla(u - I^{\omega_i}u)|^2 \preceq \int_{\omega_i} \kappa |\nabla \chi_i|^2 |(u - I^{\omega_i}u)|^2 + |\int_{\omega_i} g\chi_i^2(u - I^{\omega_i}u)|. \tag{14}$$

Similarly,

$$\int_{\omega_i^+} \kappa |\chi_i^+|^2 |\nabla(u - I^{\omega_i^+}u)|^2 \preceq \int_{\omega_i^+} \kappa |\nabla \chi_i^+|^2 |(u - I^{\omega_i^+}u)|^2 + |\int_{\omega_i^+} g|\chi_i^+|^2(u - I^{\omega_i^+}u)|. \tag{15}$$

Next, taking into account that MsFEM solution, u_H, provides a minimal energy error, we have

$$\begin{aligned}
\int_D \kappa |\nabla(u - u_H)|^2 &\preceq \int_D \kappa |\nabla(\sum_i \chi_i(u - I^{\omega_i}u))|^2 \\
&\preceq \sum_i \int_{\omega_i} \kappa |\nabla \chi_i|^2 |u - I^{\omega_i}u|^2 + \sum_i \int_{\omega_i} \kappa |\chi_i|^2 |\nabla(u - I^{\omega_i}u)|^2. \tag{16}
\end{aligned}$$

Combining this inequality with (14), we obtain,

$$\begin{aligned}
\int_D \kappa |\nabla(u - u_H)|^2 &\preceq \sum_i \int_{\omega_i} \kappa |\nabla \chi_i|^2 |u - I^{\omega_i}u|^2 + \left(\sum_i \int_{\omega_i} \kappa |\chi_i|^2 |\nabla(u - I^{\omega_i}u)|^2\right) \\
&\preceq \sum_i \int_{\omega_i} \kappa |\nabla \chi_i|^2 |u - I^{\omega_i}u|^2 + \left(\int_{\omega_i} \kappa |\nabla \chi_i|^2 |(u - I^{\omega_i}u)|^2 \right. \\
&\quad \left. + \sum_i |\int_{\omega_i} g|\chi_i|^2(u - I^{\omega_i}u)|\right) \\
&\preceq \sum_i \int_{\omega_i} \kappa |\nabla \chi_i|^2 |u - I^{\omega_i}u|^2 + \sum_i |\int_{\omega_i} g|\chi_i|^2(u - I^{\omega_i}u)| \tag{17}
\end{aligned}$$

Next, we concentrate in deriving a bound for the first term on the right hand side of the last inequality above.

Note that $I^{\omega_i^+}u = I^{\omega_i}u$ in ω_i. Next, we define the interpolant $I^{\omega_i^+}u$ using the modes for the eigenvalue problem Eq. (7) that correspond to the eigenvalues $\lambda_1^{\omega_i}, \cdots, \lambda_{L_i}^{\omega_i}$. Then, we have

$$\int_{\omega_i^+} \kappa |\nabla \chi_i^+|^2(u - I^{\omega_i^+}u)^2 \preceq \frac{1}{\lambda_{L_i+1}^{\omega_i}} \int_{\omega_i} \kappa |\nabla(u - I^{\omega_i}u)|^2, \tag{18}$$

which is easily deduced from the corresponding eigenvalue problem and the definition of the in-

terpolation $I^{\omega_i}u$, we have

$$\sum_i \int_{\omega_i} \kappa|\nabla\chi_i|^2|u - I^{\omega_i}u|^2 \preceq \sum_i \int_{\omega_i^+} \kappa|\nabla\chi_i^+|^2|u - I^{\omega_i^+}u|^2 \preceq \sum_i \frac{1}{\lambda_{L_i+1}^{\omega_i}} \int_{\omega_i} \kappa|\nabla(u - I^{\omega_i}u)|^2.$$
(19)

Note also that we can bound the last term above by

$$
\begin{aligned}
&\sum_i \frac{1}{\lambda_{L_i+1}^{\omega_i}} \int_{\omega_i} \kappa|\nabla(u - I^{\omega_i}u)|^2 \preceq \sum_i \frac{1}{\lambda_{L_i+1}^{\omega_i}} \int_{\omega_i^+} \kappa|\chi_i^+|^2|\nabla(u - I^{\omega_i^+}u)|^2 \\
\preceq\ &\sum_i \frac{1}{\lambda_{L_i+1}^{\omega_i}} \int_{\omega_i^+} \kappa|\nabla\chi_i^+|^2|u - I^{\omega_i^+}u|^2 + \sum_i \frac{1}{\lambda_{L_i+1}^{\omega_i}}|\int_{\omega_i^+} g|\chi_i^+|^2(u - I^{\omega_i^+}u)| \quad \text{(by (15))} \\
\preceq\ &\frac{1}{\Lambda_*}\left(\sum_i \int_{\omega_i^+} \kappa|\nabla\chi_i^+|^2|u - I^{\omega_i^+}u|^2 + \sum_i |\int_{\omega_i^+} g|\chi_i^+|^2(u - I^{\omega_i^+}u)|\right) \\
\preceq\ &\frac{1}{\Lambda_*}\left(\sum_i \frac{1}{\lambda_{L_i+1}^{\omega_i}} \int_{\omega_i} \kappa|\nabla(u - I^{\omega_i}u)|^2 + \sum_i |\int_{\omega_i^+} g|\chi_i^+|^2(u - I^{\omega_i^+}u)|\right), \quad \text{(by (18))}
\end{aligned}
$$

where we have defined $\Lambda_* = \min_{\omega_i} \lambda_{L_i+1}^{\omega_i}$. Thus, summarizing the last set of inequalities we obtain,

$$\sum_i \frac{1}{\lambda_{L_i+1}^{\omega_i}} \int_{\omega_i} \kappa|\nabla(u - I^{\omega_i}u)|^2 \preceq \frac{1}{\Lambda_*}\left(\sum_i \frac{1}{\lambda_{L_i+1}^{\omega_i}} \int_{\omega_i} \kappa|\nabla(u - I^{\omega_i}u)|^2 + \sum_i |\int_{\omega_i^+} g|\chi_i^+|^2(u - I^{\omega_i^+}u)|\right).$$

Applying this inequality n times in the estimate for $\sum_i \int_{\omega_i} \kappa|\nabla\chi_i|^2|u - I^{\omega_i}u|^2$ in Eq. (19), we get

$$
\begin{aligned}
&\sum_i \int_{\omega_i^+} \kappa|\nabla\chi_i^+|^2|u - I^{\omega_i^+}u|^2 \preceq \sum_i \frac{1}{\lambda_{L_i+1}^{\omega_i}} \int_{\omega_i} \kappa|\nabla(u - I^{\omega_i}u)|^2 \\
\preceq\ &\left(\frac{1}{\Lambda_*}\right)^n \sum_i \int_{\omega_i} \frac{1}{\lambda_{L_i+1}^{\omega_i}} \kappa|\nabla(u - I^{\omega_i}u)|^2 + \sum_{j=1}^{n}\left(\frac{1}{\Lambda_*}\right)^j \sum_i |\int_{\omega_i^+} g|\chi_i^+|^2(u - I^{\omega_i^+}u)| \\
\preceq\ &\left(\frac{1}{\Lambda_*}\right)^{n+1} \sum_i \int_{\omega_i} \kappa|\nabla(u - I^{\omega_i}u)|^2 + (\Lambda_*)^n\left(\frac{1 - \Lambda_*^{-n}}{\Lambda_* - 1}\right) \sum_i \int_{\omega_i^+} (|\kappa||\nabla\chi_i^+|^2)^{-1}g^2.
\end{aligned}
$$

Considering $\sum_i \int_{\omega_i} \kappa|\nabla(u - I^{\omega_i}u)|^2 \preceq \int_D \kappa|\nabla u|^2$, we have the following convergence rate for GMsFEM,

$$\int_D \kappa|\nabla(u - u_H)|^2 \preceq \frac{1}{\Lambda_*^{n+1}} \int_D \kappa|\nabla u|^2 + \left((\Lambda_*)^n\left(\frac{1 - \Lambda_*^{-n}}{\Lambda_* - 1}\right) + 1\right)R,$$
(20)

where $R = \sum_i \int_{\omega_i^+} (|\kappa||\nabla\chi_i^+|^2)^{-1} g^2$. For right hand sides with $g \preceq 1$ it can be shown that $\int_{\omega_i^+} \left(\kappa|\nabla\chi_i^+|^2\right)^{-1} g^2 \preceq H^2$.

With this assumption, we have the convergence result,

$$\int_D \kappa|\nabla(u - u_H)|^2 \preceq \frac{1}{\Lambda_*^{n+1}} \int_D \kappa|\nabla u|^2 + \left((\Lambda_*)^n \left(\frac{1 - \Lambda_*^{-n}}{\Lambda_* - 1}\right) + 1\right) H^2 \int_D |1|^2. \qquad (21)$$

Choosing Λ_* sufficiently large (larger than 1) and $n = 1 - \frac{\log(H)}{\log\Lambda_*}$ (in each ω_i), we obtain

$$\int_D \kappa|\nabla(u - u_H)|^2 \preceq \left(\frac{H}{\Lambda_*}\right) \int_D \kappa|\nabla u|^2 + \frac{H}{\Lambda_*}. \qquad (22)$$

Collecting the results above, we have

Theorem 3. *If $\Lambda_* \geq 1$ and $\int_D \kappa^{-1}g^2 \preceq 1$, then*

$$\int_D \kappa|\nabla(u - u_H)|^2 \preceq \left(\frac{H}{\Lambda_*}\right) \int_D \kappa|\nabla u|^2 + \frac{H}{\Lambda_*}.$$

Next, we comment on the estimate on g. We consider the snapshot space generated by Eq. (4). Because $|\nabla\chi_i^+|^2 \preceq H^{-2}$, we have $R \preceq H^2 \int_{\omega_i^+} \kappa^{-1}g^2$. We assume that $I^{\omega_i^+} u = \sum_{l=1}^L c_l\Psi_l$, where Ψ_l are eigenvectors Eq. (8). Each eigenvector Ψ_l is spanned by eigenvectors of Eq. (4), i.e., $\Psi_l = d_{lm}\psi_m^+$. Then, $g = f + \text{div}(\kappa(x)\nabla I^{\omega_i}u) = f - \sum_{m=1}^{M_{\text{snap}}} \sum_{l=1}^L c_l d_{lm}\lambda_m\kappa\psi_m^+ = f - \sum_m d_m^*\lambda_m\kappa\psi_m^+$, where $d_{m,L}^* = \sum_{l=1}^L c_l d_{lm}$, λ_m are eigenvalues in Eq. (4), M_{snap} is the number of snapshots, and L is the number of modes selected in the offline stage. Due to orthogonality of ψ_m^+, it can be shown that $\int_{\omega_i^+} \kappa^{-1}g^2 \preceq 1 + \sum_m (d_{m,L}^*)^2\lambda_m^2$, provided $1 \preceq \kappa$. On the other hand, $\int_{\omega_i^+} \kappa|\nabla I^{\omega_i^+}u|^2 = \sum_m (d_{m,L}^*)^2\lambda_m$. Thus,

$$\int_{\omega_i^+} \kappa^{-1}g^2 \preceq 1 + \Lambda_*^{\text{snap}} \int_{\omega_i^+} \kappa|\nabla I^{\omega_i^+}u|^2.$$

5.2. Offline space using multiple spectral problems and the relation to oversampled spectral problems

In this subsection we briefly consider the convergence analysis for the offline space proposed in Section 3.2.2. For this analysis we use the harmonic snapshot space to avoid any residual error, though the derivation can be extended to other scenarios. This derivation uses the proof of Theorem 3.3 from the work of Babuška and Lipton [4] and we extend it to a high-contrast case. We start with the inequality in Eq. (17). We define two interpolants $I^{\omega_i^+}u$ and $I^{\omega_i}u$ by choosing the dominant

modes through considering

$$\int_{\omega_i^+} \kappa |\nabla \chi_i^+|^2 (u - I^{\omega_i^+} u)^2 \preceq \frac{1}{\lambda_{L_i+1}^{\omega_i^+}} \int_{\omega_i^+} \kappa |\nabla (u - I^{\omega_i^+} u)|^2 \preceq \frac{1}{\lambda_{L_i+1}^{\omega_i^+}} \int_{\omega_i^+} \kappa |\nabla u|^2 \qquad (23)$$

$$\int_{\omega_i} \kappa |\nabla \chi_i|^2 (\widehat{u} - I^{\omega_i} \widehat{u})^2 \preceq \frac{1}{\lambda_{L_i+1}^{\omega_i}} \int_{\omega_i} \kappa |\nabla (\widehat{u} - I^{\omega_i} \widehat{u})|^2 \preceq \frac{1}{\lambda_{L_i+1}^{\omega_i}} \int_{\omega_i} \kappa |\nabla \widehat{u}|^2, \qquad (24)$$

where $\widehat{u} = u - I^{\omega_i^+} u$, $\frac{1}{\lambda_{L_i+1}^{\omega_i^+}}$ and $\frac{1}{\lambda_{L_i+1}^{\omega_i}}$ are sufficiently small. We choose the interpolant to be $I^{\omega_i^+} u + I^{\omega_i} \widehat{u}$. Thus, $u - (I^{\omega_i^+} u + I^{\omega_i} \widehat{u}) = \widehat{u} - I^{\omega_i} \widehat{u}$. Then, we have

$$\sum_i \int_{\omega_i} \kappa |\nabla \chi_i|^2 |\widehat{u} - I^{\omega_i} \widehat{u}|^2 \preceq \sum_i \frac{1}{\lambda_{L_i+1}^{\omega_i}} \int_{\omega_i} \kappa |\nabla (\widehat{u} - I^{\omega_i} \widehat{u})|^2$$

$$\preceq \sum_i \frac{1}{\lambda_{L_i+1}^{\omega_i}} \int_{\omega_i^+} \kappa |\chi_i^+|^2 |\nabla (\widehat{u} - I^{\omega_i^+} \widehat{u})|^2 \preceq \sum_i \frac{1}{\lambda_{L_i+1}^{\omega_i}} \int_{\omega_i^+} \kappa |\nabla \chi_i^+|^2 |\widehat{u} - I^{\omega_i^+} \widehat{u}|^2$$

$$\preceq \frac{1}{\Lambda_*} \left(\sum_i \int_{\omega_i^+} \kappa |\nabla \chi_i^+|^2 |\widehat{u}|^2 \right)$$

$$\preceq \frac{1}{\Lambda_*} \left(\sum_i \frac{1}{\lambda_{L_i+1}^{\omega_i^+}} \int_{\omega_i^+} \kappa |\nabla (u - I^{\omega_i} u)|^2 \right) \preceq \frac{1}{\Lambda_*} \frac{1}{\Lambda_*^+} \int_D \kappa |\nabla u|^2, \qquad (25)$$

where $\Lambda_* = \min_{\omega_i} \lambda_{L_i+1}^{\omega_i}$ and $\Lambda_*^+ = \min_{\omega_i} \lambda_{L_i+1}^{\omega_i^+}$. Thus, choosing Λ_* and Λ_*^+ to be sufficiently large, the convergence rate can be improved. In particular, the final estimates involve the product of the convergence rates with individual spaces.

The above results can be summarized in the following way. If Eq. (23) and Eq. (24) can be satisfied by choosing appropriate interpolants in ω and ω^+, then

$$\int_D \kappa |\nabla (u - u_H)|^2 \preceq \frac{1}{\Lambda_*} \frac{1}{\Lambda_*^+} \int_D \kappa |\nabla u|^2.$$

This result can easily be extended to use multiple eigenvalue problems (instead of two eigenvalue problems).

Remark 4. *In the above proof, we rely on the estimates that bound the L_κ^2-norm via the H_κ^1-norm in ω and ω^+. In addition, we use an inequality that bounds $H_\kappa^1(\omega)$ by $L_\kappa^2(\omega^+)$ norms based on PDE estimates. The latter can be replaced by a third eigenvalue problem, $A^{+,off} \Psi_k^{off} = \lambda_k^{off} S^{off} \Psi_k^{off}$, (cf. Eq. (7)), and one can select its important modes (corresponding to largest eigenvalues) to reduce the constant relating $H_\kappa^1(\omega)$ to $L_\kappa^2(\omega^+)$ norms. We have implemented this procedure and*

observed a slight improvement, at the cost of additional basis functions (similar to the numerical results presented in Section 4.1.1).

Next, we discuss the relation of using multiple spectral problems to the eigenvalue problems discussed earlier. Because of the optimality of local spectral spaces (cf. [4] and see below), we know that the spectral problems that are similar to those described by Eqs. (7) and (8) will provide a better convergence rate compared to those using multiple spectral problems. For the two spectral problems described above, one can equivalently use (cf. Eqs. (7) and (8)) the following local spectral problem

$$A^{+,\text{off}}\Psi_k^{\text{off}} = \lambda_k^{\text{off}} S^{\text{off}}\Psi_k^{\text{off}} \tag{26}$$

for construction of the offline spaces. Indeed, if Eq. (26) is used, we can show that (cf. Eq. (25))

$$\sum_i \int_{\omega_i} \kappa|\nabla\chi_i|^2|u - I^{\omega_i}u|^2 \preceq \sum_i \frac{1}{\widetilde{\lambda}_{L_i+1}^{\omega_i^+}} \int_{\omega_i^+} \kappa|\nabla(u - I^{\omega_i}u)|^2 \preceq \frac{1}{\widetilde{\Lambda}_*} \int_D \kappa|\nabla u|^2, \tag{27}$$

where $\widetilde{\Lambda}_* = \min_{\omega_i}\widetilde{\lambda}_{L_i+1}^{\omega_i}$. On the other hand, the local spectral problem Eq. (26) provides an optimal subspace in the following sense. For a fixed L_i dimensional subspace in ω_i, a space that provides the smallest

$$\max_u \min_{u_0} \frac{(u - u_0)^T S^{\text{off}}(u - u_0)}{(u - u_0)^T A^{+,\text{off}}(u - u_0)}$$

is given by the the the span of the smallest (in terms of corresponding eigenvalues) L_i eigenvectors of Eq. (26) (see also [4] for more general discussions), or by the largest (in terms of corresponding eigenvalues) L_i eigenvectors of $S^{+,\text{off}}\Psi_k^{\text{off}} = \left(\lambda_k^{\text{off}}\right)^{-1} A^{\text{off}}\Psi_k^{\text{off}}$. Consequently, the use of Eq. (26) in constructing local spaces will give a better approximation compared to using multiple spectral problems that provides a rate which is the product of $\prod_j 1/\Lambda_{*,j}$, where j represents the corresponding eigenvalue for j-th eigenvalue problem. Consequently, if we set a threshold for the eigenvalue for each problem as Λ_*, then the convergence rate is $(1/\Lambda_*)^n$, where n is the number of eigenvalue problems are used. Note also that, each used eigenvalue problem will increase the dimension of the final reduced space. In general, one can show similar results for eigenvalue problems considered earlier, as in Eqs. (7) and (8).

We present numerical results corresponding to the use of the eigenvalue problem in Eq. (26) in Table 17. If we compare these results to Table 7, we observe that the convergence of the method is better than if the eigenvalue problem of Eq. (8) is used.

$\dim(V_{\text{off}}^+)$	Λ_*	$\|u - u^{+,\text{off}}\|$ (%)	
		$L_\kappa^2(D)$	$H_\kappa^1(D)$
1163	3.01×10^3	3.11	34.53
1524	5.35×10^3	0.25	13.64
1885	7.51×10^3	0.20	8.69
2607	7.76×10^3	0.12	5.91

Table 17: Relative errors between the fine scale solution and **offline spaces** obtained from using oversampled domains; Eigenvalue problem from Eq. (26), 20×20 coarse mesh, harmonic snapshots, $\omega_i^+ = 3 \times \omega_i$.

6. Conclusions

In this paper, we develop and investigate oversampling strategies for GMsFEM. The GMsFEM offers a flexible framework for solving multiscale problems by constructing a reduced dimensional approximation for the solution space. In particular, GMsFEM constructs a local approximation space via appropriate local spectral problems. We show that the use of oversampling strategies can yield a convergence independent of the contrast and the small scales under certain assumptions. The proof relies on the fact that the local spectral problems that are used for basis construction involve oversampled regions. The convergence of GMsFEM is proportional to the maximum of the inverse of the eigenvalue such that the corresponding eigenvector is not included in the coarse space. Our numerical results show that the reciprocal of the eigenvalues decay faster when over-sampling is used (in particular, for the local spectral problem that is proposed in the paper). We present some representative numerical results where various oversampling strategies are studied. Our results compare the fine grid solution with GMsFEM solution as well as the solution computed in the snapshot space with GMsFEM solution. We study the use of multiple spectral problems for enhanced accuracy and discuss their relation to single spectral problems that use oversampled regions where the latter provides an optimal space. Both convergence analysis and numerical studies are presented. Numerical results show that the proposed oversampling techniques are efficient and have similar errors. We also present numerical results for parameter-dependent problems using our proposed strategies. The numerical results for each configuration are discussed in the paper.

References

[1] J. E. Aarnes, *On the use of a mixed multiscale finite element method for greater flexibility and increased speed or improved accuracy in reservoir simulation*, SIAM J. Multiscale Modeling and Simulation, 2 (2004), 421-439.

[2] J. E. Aarnes, S. Krogstad, and K.-A. Lie, *A hierarchical multiscale method for two-phase flow based upon mixed finite elements and nonuniform grids*, Multiscale Model. Simul. 5(2) (2006), pp. 337–363.

[3] T. Arbogast, G. Pencheva, M. F. Wheeler, and I. Yotov, *A multiscale mortar mixed finite element method*, SIAM J. Multiscale Modeling and Simulation, 6(1), 2007, 319-346.

[4] I. Babuška and R. Lipton, *Optimal Local Approximation Spaces for Generalized Finite Element Methods with Application to Multiscale Problems*. Multiscale Modeling and Simulation, SIAM 9 (2011) 373-406.

[5] I. Babuška and E. Osborn, *Generalized Finite Element Methods: Their Performance and Their Relation to Mixed Methods,* SIAM J. Numer. Anal., 20 (1983), pp. 510-536.

[6] L. Berlyand and H. Owhadi, *Flux norm approach to finite dimensional homogenization approximations with non-separated scales and high contrast*, Arch. Ration. Mech. Anal., 198 (2010), pp. 677-721.

[7] S. Boyaval, C. LeBris, T. Lelièvre, Y. Maday, N. Nguyen, and A. Patera, *Reduced Basis Techniques for Stochastic Problems*, Archives of Computational Methods in Engineering, 17:435-454, 2010.

[8] Y. Chen and L. Durlofsky, *An ensemble level upscaling approach for efficient estimation of fine-scale production statistics using coarse-scale simulations*, SPE paper 106086, presented at the SPE Reservoir Simulation Symposium, Houston, Feb. 26-28 (2007).

[9] Y. Chen, L.J. Durlofsky, M. Gerritsen, and X.H. Wen, *A coupled local-global upscaling approach for simulating flow in highly heterogeneous formations*, Advances in Water Resources, 26 (2003), pp. 1041–1060.

[10] Y. Efendiev, J. Galvis, R. Lazarov, M. Moon, M. Sarkis, *Generalized Multiscale Finite Element Method. Symmetric Interior Penalty Coupling*, Submitted.

[11] Y. Efendiev, J. Galvis, R. Lazarov, and J. Willems, *Robust domain decomposition preconditioners for abstract symmetric positive definite bilinear forms*, ESAIM: Mathematical Modelling and Numerical Analysis, September 2012, 46, pp. 1175-1199.

[12] Y. Efendiev, J. Galvis, and T. Hou, *Generalized Multiscale Finite Element Methods*, Submitted. http://arxiv.org/submit/631572.

[13] Y. Efendiev, J. Galvis, and F. Thomines, *A systematic coarse-scale model reduction technique for parameter-dependent flows in highly heterogeneous media and its applications*, SIAM MMS 10(4), 1317-1343, 2012.

[14] Y. Efendiev, J. Galvis, and X. H. Wu, *Multiscale finite element methods for high-contrast problems using local spectral basis functions*, Journal of Computational Physics. Volume 230, Issue 4, 20 February 2011, Pages 937-955.

[15] Y. Efendiev, V. Ginting, T. Hou, and R. Ewing, *Accurate multiscale finite element methods for two-phase flow simulations*, J. Comp. Physics, 220 (1), pp. 155–174, 2006.

[16] Y. Efendiev and T. Hou, *Multiscale finite element methods. Theory and applications*, Springer, 2009.

[17] Y. Efendiev, T. Hou, and V. Ginting. *Multiscale finite element methods for nonlinear problems and their applications*. Comm. Math. Sci., 2:553179, 2004.

[18] J. Galvis and Y. Efendiev, *Domain decomposition preconditioners for multiscale flows in high-contrast media: Reduced dimension coarse spaces*, SIAM J. Multiscale Modeling and Simulation, Volume 8, Issue 5, 1621-1644 (2010).

[19] T.Y. Hou and X.H. Wu, *A multiscale finite element method for elliptic problems in composite materials and porous media*, Journal of Computational Physics, 134 (1997), 169-189.

[20] T. Hughes, G. Feijoo, L. Mazzei, and J. Quincy, *The variational multiscale method - a paradigm for computational mechanics*, Comput. Methods Appl. Mech. Engrg, 166 (1998), 3-24.

[21] P. Jenny, S.H. Lee, and H. Tchelepi, *Multi-scale finite volume method for elliptic problems in subsurface flow simulation*, J. Comput. Phys., 187 (2003), 47-67.

[22] M.A. Grepl, Y. Maday, N.C. Nguyen, and A.T. Patera. *Efficient reduced-basis treatment of non-affine and nonlinear partial differential equations*. ESIAM : M2AN, 41(2):575175, 2007.

[23] G. Rozza, D. B. P Huynh, and A. T. Patera, *Reduced basis approximation and a posteriori error estimation for affinely parametrized elliptic coercive partial differential equations. Application to transport and continuum mechanics*. Arch Comput Methods Eng 15(3):229?275, 2008.